Superconductivity, magnetic fluctuations, and magnetic order in $TbSr_2Cu_{2.69}Mo_{0.31}O_7$

W.-H. Li, W. Y. Chuang, S. Y. Wu, and K. C. Lee
Department of Physics, National Central University, Chung-Li, Taiwan 32054, Republic of China

J. W. Lynn
Reactor Radiation Division, NIST, Gaithersburg, Maryland 20899

H. L. Tsay and H. D. Yang
Department of Physics, National Sun Yat-Sen University, Kaohsiung, Taiwan 80424, Republic of China

(Received 6 February 1997)

Neutron-diffraction and ac-susceptibility measurements have been performed to study the superconductivity and magnetic order of the Tb spins in polycrystalline $TbSr_2Cu_{2.69}Mo_{0.31}O_7$. Superconductivity with an onset temperature at 37 K was observed in the dc electrical resistivity and ac-magnetic-susceptibility measurements. A two-step transition to the superconducting state was seen, as both intragranular and Josephson-like intergranular losses were evident in the out-of-phase component of the ac susceptibility. Magnetic correlations between the Tb spins start developing around 40 K, and the correlation length diverges at $T_N = 5.4$ K with the nearest-neighbor Tb spins aligned antiparallel along all three crystallographic directions. Below 5.4 K, superconductivity and Tb magnetic order coexist. [S0163-1829(97)01834-1]

I. INTRODUCTION

The superconducting and magnetic properties of the rare-earth doped high-T_c layered compounds $RBa_2Cu_3O_{6+x}$(R-123) have been intensively studied for all R = rare earth but Ce, Pm, and Tb. Although the presence of the local f moments of the R ions (expect that of Pr) is found to have little influence on the superconducting properties of the systems, the magnetic properties of the R ions are quite different from one R to another.[1–4] Various types of ordering of the R sublattice have been observed from three-dimensional (3D) long-range order to two-dimensional (2D) short-range correlations persisting to temperatures well above the ordering temperature. The failure to form Ba-based Ce-123, Pm-123, and Tb-123 systems unfortunately precludes the study of the interplay between these R magnetism and the superconductivity in these systems. Among them, the formation of the stable $TbBaO_3$ phase in the sample preparation process is now generally believed to be the main reason preventing the formation of $TbBa_2Cu_3O_{6+x}$.[5,6] Apparently, using the chemically similar element Sr to replace Ba is an alternative, since no stable $TbSrO_3$ may form to inhibit the formation of $TbSr_2Cu_3O_{6+x}$. Recently, Sr-based Tb-123 compounds[7] have been successfully synthesized,[8,9] but partially substituting Mo for the Cu in the CuO-chain layers is also needed to stabilize the structure. The instability is believed to arise from the replacement of the smaller Sr for Ba that results in lattice mismatches among constituent elements.[10]

So far only a few Tb-based compounds have been studied in detail. Among them the magnetic interactions between the Tb spins in $Pb_2Sr_2TbCu_3O_8$ have been found[11,12] to be two-dimensional and antiferromagnetic (AF) in nature. The Tb spins order with a relatively high ordering temperature of $T_N = 5.3$ K, and the 2D short-range correlations among the Tb spins were directly observed[11,12] by neutron diffraction to persist up to ~ 10 K. Inelastic-neutron-scattering and magnetic-susceptibility measurements[6] further suggest that significant Tb spin correlations persist up to temperatures as high as 120 K, which is more than 20 times T_N. All these observations indicate that the couplings between the Tb spins are relatively strong. In addition, the Tb moments are usually sizable, which provides a better experimental situation for studying the magnetic fluctuations above the ordering temperature if they do exist. In this article, we report the superconductivity and magnetic ordering of the Tb spins observed in a Sr-based Tb-123 compound studied using dc electrical resistivity, ac magnetic susceptibility, and neutron-diffraction measurements. The crystal structure obtained by refining the high-resolution neutron-diffraction pattern shows that the compound has a composition of $TbSr_2Cu_{2.69}Mo_{0.31}O_7$, with the Mo atoms replacing the Cu atoms in the CuO-chain layers. Both superconductivity and magnetic correlations between the Tb spins were observed to develop around 40 K. Zero resistivity occurs at $T_c = 32$ K, while the Tb spins order antiferromagnetically along all three crystallographic directions at $T_N = 5.4$ K. Below 5.4 K, superconductivity within the CuO_2-plane layers and 3D long-range order of the Tb spins located between the CuO_2-plane layers coexist.

II. CRYSTAL STRUCTURE

About 11 g of polycrystalline $TbSr_2Cu_{2.69}Mo_{0.31}O_7$ was prepared by the standard solid-state reaction technique. Stoichiometric amounts of high-purity Tb_4O_7, $SrCO_3$, MoO_3, and CuO were mixed and pressed into pellets. The mixed powders were heated at 1020 °C for 3 h in an oxygen atmosphere, and then slowly cooled to room temperature in flowing oxygen. This process was repeated three times to obtain a more homogeneous sample. X-ray diffraction was first used to characterize the sample pellet by pellet. No obvious differences were observed among the x-ray-diffraction patterns taken on different pellets, which all can be well de-

TABLE I. Structural parameters and selected bond distances for $TbSr_2Cu_{2.69}Mo_{0.31}O_7$ at room temperature ($Pmmm$).

Atom	Structure coordinates X	Y	Z	Occup.	Bond distance Bond atoms	Distance (Å)
Tb	0.5000	0.5000	0.5000	1	Tb-O(2)	2.44753
Sr	0.5000	0.5000	0.1926(3)	2	Cu(2)-O(1)	2.24811
Cu(1)	0.0000	0.0000	0.0000	0.69(3)	Cu(2)-O(2)	1.92108
Mo	0.0000	0.0000	0.0000	0.31(3)	Mo-O(1)	1.84031
Cu(2)	0.0000	0.0000	0.3539(3)	2	Cu(2)-O(3)	1.92661
O(1)	0.0000	0.0000	0.1593(2)	2	Sr-O(1)	2.7325
O(2)	0.5000	0.0000	0.3688(2)	2	Sr-O(2)	2.7936
O(3)	0.0000	0.5000	0.3740(3)	2	Sr-O(3)	2.8376
O(4)	0.0000	0.5000	0.0121(4)	0.997(1)	Si-O(4)	2.8300
R_p (%) = 7.88		R_{wp} (%) = 10.14		$\chi^2 = 5.532$		
$a = 3.82671(4)$ Å		$b = 3.82516(4)$ Å		$c = 11.55249(7)$ Å		

scribed by the $YBa_2Cu_3O_{6+x}$ structure.[13] The precise nuclear structure was then obtained by a complete structural analysis using neutron diffraction. A high-resolution neutron-diffraction pattern covering the range of scattering angle $3° \leqslant 2\theta \leqslant 140°$ taken at room temperature was collected on BT-1, the 32-detector powder diffractometer at the Research Reactor at the U.S. National Institute of Standards and Technology (NIST). The neutrons had a wavelength of $\lambda = 1.5454$ Å defined by a Cu(311) monochromator. Angular collimations used before and after the monochromator position, and after the sample position were, respectively, 15′-20′-7′ full width at half maximum (FWHM).

The diffraction pattern was analyzed using the General Structure Analysis System (GSAS) program of Larson and Von Dreele,[14] in which the Rietveld refinement method[15,16] was followed. In the refinement, the portions of the diffraction pattern containing peaks from the aluminum can used to hold the sample were excluded. All peaks are described well by Gaussian peak profiles. The refinement was carried out assuming the symmetry of space group Pmmm, using the parameters found in Ref. 13 for Y-123 as the initial parameters, with the Mo atoms located in the CuO-chain layers. Models allowing the Mo atoms to be present in the CuO_2-plane layers gave unacceptable negative occupancy factors for Mo and for the chain Cu. The starting lattice parameters for the refinement were determined from least-square analysis of the x-ray pattern. All structural and lattice parameters were allowed to vary simultaneously until R_w, the weighted R factor,[14] differed by less than one part in a thousand in two successive cycles. Careful analysis of the occupancy factors of the oxygen atoms shows that the oxygen sites in the (Cu/Mo)O-chain layers are almost full with an oxygen content of 6.97(2) for the compound. Table I lists the final structural parameters and selected bond distances. The observed and calculated patterns are shown in Fig. 1, where the short vertical lines shown below the pattern indicate the angular positions of the Bragg reflections expected by the structure listed in Table I. Only a few additional very weak lines were present, showing the compound is practically single phase. We estimated that impurity phases in the sample are about 3%. At the bottom of Fig. 1, we show the difference between the calculated and the observed patterns. The agreement between the calculated and observed patterns is quite good, showing that the observed pattern can be described well by the proposed structure. The Mo replaced the Cu in the CuO-chain layers with a refined content of 0.31, which gives a chemical formula of $TbSr_2Cu_{2.69}Mo_{0.31}O_{6.97}$ for the compound. However, a relatively large value of ± 0.03 was obtained for the uncertainty of the Mo content. This is mainly because the neutron-scattering amplitudes for

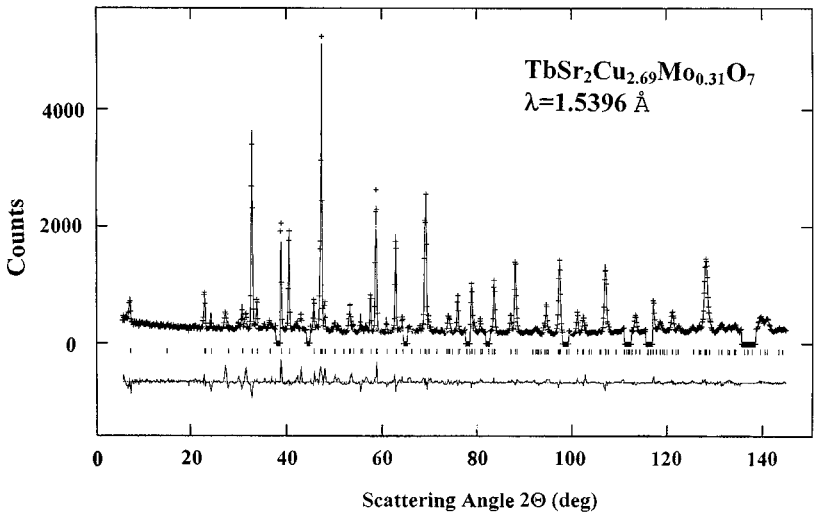

FIG. 1. Observed (crosses) and fitted (solid lines) high-resolution neutron-powder-diffraction pattern taken at room temperature. The vertical lines shown below the pattern mark the calculated positions of nuclear Bragg reflections. The differences between the observed and calculated patterns are also plotted at the bottom.

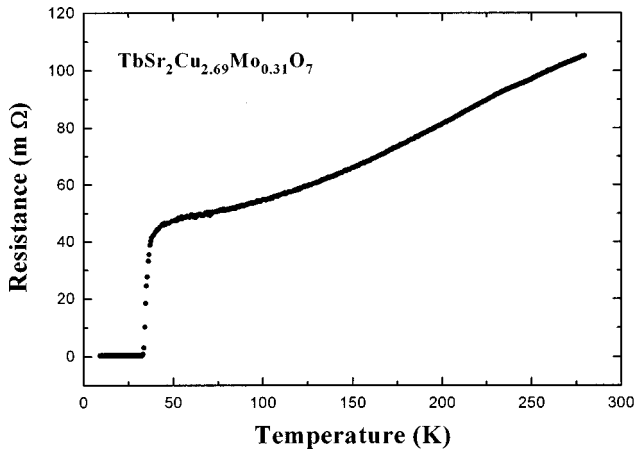

FIG. 2. Temperature dependence of the dc electrical resistance. A sharp drop is evident starting at $T=37$ K and zero resistance is achieved at $T=32$ K, showing the occurrence of superconductivity.

Cu and Mo differ by only 10% [b(Cu)$=0.7718$ and b(Mo) $=0.695$],[17] which reduces the ability to resolve Cu and Mo by neutrons.

III. SUPERCONDUCTIVITY

In Fig. 2 we show the variation of the dc electrical resistance $R(T)$ with temperature, where the data were obtained employing the standard four-probe method. The resistance decreases monotonically as temperature is reduced, showing metallic behavior. A sharp drop starting at $T=37$ K is evident, and zero resistance is achieved at $T=32$ K. This zero-resistance state remains down to 4.3 K, the lowest temperature studied. Below 32 K the system exhibits superconductivity, which is also evident in the temperature dependence of the ac susceptibility shown in Fig. 3, where χ' and χ'' denote the in-phase and the out-of-phase components, respectively. Above 40 K, $\chi'(T)$ can be described by the sum of a small temperature independent term χ_0' and a Curie-Weiss contribution for antiferromagnetic systems

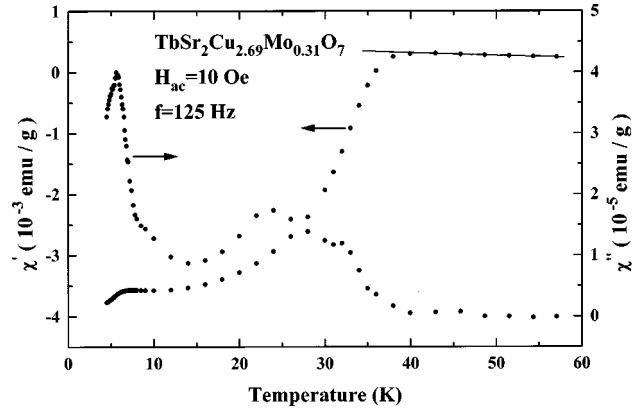

FIG. 3. Low-temperature portions of the variation of χ' and χ'' with temperature. Below 40 K, a diamagnetic response showing the occurrence of superconductivity is clearly seen in the $\chi'(T)$ curve. The peaks at 32 and 24 K in χ'' are associated, respectively, with the intragranular and intergranular losses during the superconducting transition. The peak at 5.4 K in χ'' corresponds to the ordering of the Tb spins.

$C/(T+\theta)$, while essentially zero values were obtained for χ''. We note that the absolute values obtained for χ' are of the order of 10^{-3} emu/g, showing that the paramagnetic response of the compound to applied field is relatively large, as expected for Tb-based systems. The solid curve shown in Fig. 3 is an extrapolation of a fit to $\chi'(T)$ obtained for the $\chi'(T)$ data between 60 and 325 K (not shown) to the expression $\chi_0'+C/(T+\theta)$ with $\theta=7.66$ K and a fitted effective moment $\mu_{\rm eff}=9.31(5)\mu_B$. We note that $9.72\mu_B$ is the value of the free ion moment for Tb^{3+}. $\chi'(T)$ is seen to depart from the Curie-Weiss curve as the temperature approaches 40 K, below which $\chi'(T)$ shows a downturn and negative values were obtained at lower temperatures. The diamagnetic response observed in $\chi'(T)$ signifies again the occurrence of superconductivity, which is also evident in $\chi''(T)$ where a two-component dissipation peak develops. Since our measurements were performed on a polycrystalline specimen, it consists of grains connected by weak links. Both the intragranular shielding current flow within the individual grains and the intergranular current flow in loops through Josephson junctions at the boundaries between grains can contribute to the ac susceptibility. The peaks at 32 and 24 K observed in $\chi''(T)$ shown in Fig. 3 are associated with the losses occurring within the grains (intragranular) and at the Josephson-like weak links (intergranular),[18–21] respectively. A two-step transition to the superconducting state is hence observed in the present studies. However, this two-step transition is not evident in the $\chi'(T)$ data. We further remark that the peak position of the intragranular loss matches the temperature at which the resistivity drops to zero. This occurrence may be understood easier if we first consider the system to be at a low temperature where the flux is fully excluded from the grains. The contribution to χ'' from the intragranular component is then small. As the field begins to penetrate into the grains at higher temperatures, the intragranular χ'' begins to vary. It peaks when the ac field penetrates into the grains completely. Above this temperature less and less of the grain volume remains superconducting, and nonzero values for the resistivity are then expected.

A second peak in $\chi''(T)$ is clearly seen at lower temperatures. This peak, centered at $T=5.4$ K, is better defined, in comparison with the superconducting peak observed at higher temperatures, and is associated with the losses occurring as the Tb spins order. Its peak position matches the ordering temperature of the Tb spins determined from neutron-diffraction measurements (see below). As the Tb spins order, the screening current is observed to increase as a second drop in $\chi'(T)$ starting around $T=7$ K is also evident in Fig. 3. In addition, zero values for the resistivity were obtained at these temperatures (see Fig. 2). These results lead to the conclusion that superconductivity and antiferromagnetic order of the Tb spins coexist below 5.4 K, and this coexistence is observed to remain down to 2.8 K, the lowest temperature achieved in the ac-susceptibility measurements.

IV. Tb ORDERING

The magnetic-neutron-diffraction experiments were conducted using the BT-2 triple-axis spectrometer at the NIST reactor. The incoming neutrons had a wavelength of 2.351 Å (14.8 meV) defined by a pyrolytic graphite PG(002) crystal,

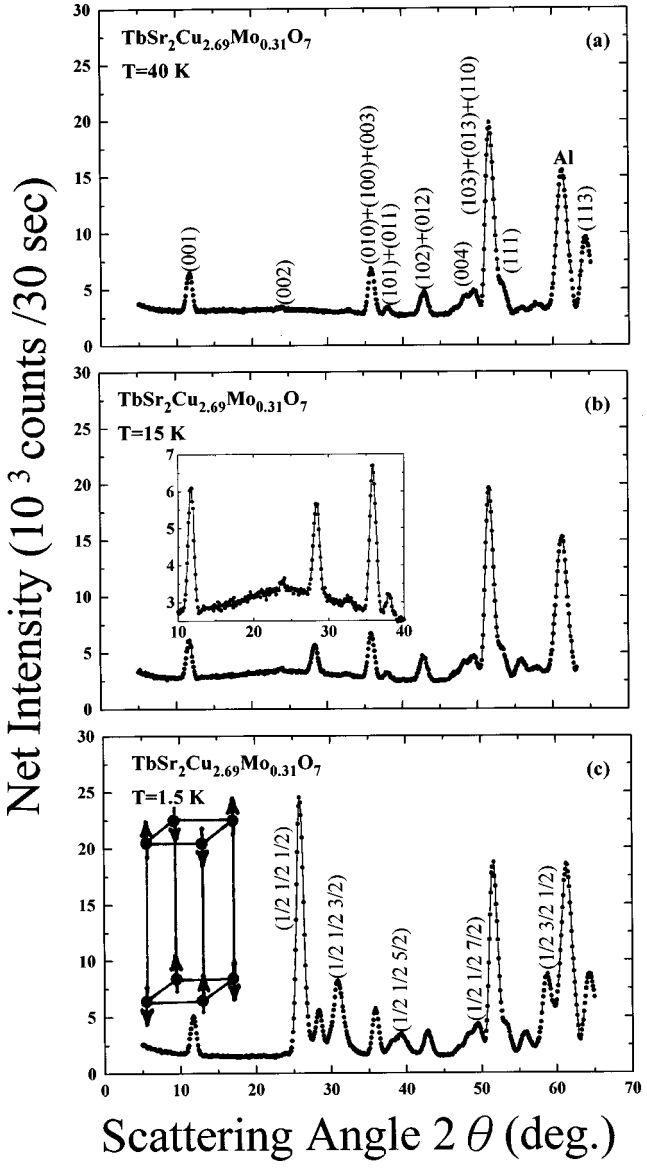

FIG. 4. Diffraction patterns taken at (a) 40 K, (b) 15 K, and (c) 1.5 K. No new peaks were observed at 40 K as compared with those observed at room temperature. At 15 K a broad peak centered at $2\theta \approx 26°$, which originates from short-range Tb spin correlations, is evident as shown in the inset of (b). This broad peak evolves into a series of resolution-limited peaks as temperature is further reduced. The indices shown in (c) are based on the nuclear unit cell. The proposed structure for the Tb spin is shown in the inset of (c).

with a PG filter placed before the monochromator position to suppress higher order wavelength contaminations. Three horizontal angular collimators of 60′-40′-40′ FWHM acceptance, were placed before and after the monochromator position and after the sample position. No analyzer crystal was used. The sample was mounted in a cylindrical aluminum can filled with helium exchange gas to facilitate thermal conduction, and a pumped ^{4}He cryostat was used to cool the sample.

Twelve sets of diffraction patterns were taken over a temperature range of $1.5\ \mathrm{K} \leqslant T \leqslant 40\ \mathrm{K}$. In Figs. 4(a), 4(b), and 4(c) we show the diffraction patterns collected at $T = 40$, 15, and 1.5 K, respectively. The resolution-limited diffraction peaks observed at $T = 40$ K may all be indexed (as marked) according to the nuclear structure discussed above. The solid curves shown in Fig. 4(a) are fits of the data to the Gaussian instrumental resolution function. No new peaks were observed at 40 K as compared with the peaks at room temperature. We note that the peak at $2\theta = 61.3°$ is the Al(111) peak from the sample can. No detectable changes of structure are observed in going from room temperature to 40 K. As the temperature is reduced to 15 K, two types of new peaks that have very different profiles develop. (1) A very broad peak covering a range in scattering angle from 10° to 40°, with the maximum intensity occurring at $2\theta \approx 26°$, as shown in the inset of Fig. 4(b) where an expanded y scale is used. Based on the nuclear unit cell this broad peak may be indexed as the $\{\frac{1}{2}\frac{1}{2}\frac{1}{2}\}$ reflection, which originates from the short-range Tb spin correlations. The details concerning this issue will be discussed below. (2) Two well-defined peaks appear at $2\theta = 28.3°$ and 55.9°, as marked by arrows in Fig. 4(b). These two peaks are resolution limited. They cannot be indexed using simple Miller indices according to the nuclear unit cell. Diffraction patterns taken at different temperatures through the peak at $2\theta = 28.3°$ show that this peak starts to develop at $T \approx 40$ K and its intensity saturated at $T \approx 10$ K. The origin of these two peaks is not clear to us at the present time. We, however, believe they may not be associated with the Tb spins in the primary compound.

Reducing the temperature further, the broad peak at $2\theta = 26°$ develops into several well-defined peaks. At $T = 1.5$ K, resolution-limited peaks that may be indexed as the $\{\frac{1}{2}\frac{1}{2}\frac{1}{2}\}$, $\{\frac{1}{2}\frac{1}{2}\frac{3}{2}\}$, $\{\frac{1}{2}\frac{1}{2}\frac{5}{2}\}$, $\{\frac{1}{2}\frac{1}{2}\frac{7}{2}\}$, and $\{\frac{1}{2}\frac{3}{2}\frac{1}{2}\}$ reflections appear, as shown in Fig. 4(c). These reflections are associated with the ordering of the Tb spins. They are symmetrical, showing that the Tb spins order three dimensionally. Half-integer indices for the magnetic peaks mean the magnetic unit cell is double the nuclear one. The nearest-neighbor Tb spins are hence aligned antiparallel along all three crystallographic directions. Moreover, the relative intensities of the magnetic peaks are consistent with the Tb moments directed along the c axis. In the inset of Fig. 4(c) we show the proposed structure of the Tb spins, where we have used the coordinate system with the Tb atoms located at the origin and only the Tb ions are shown. This is the same spin structure as the Pr and Nd ordering in the corresponding $R\mathrm{Ba_2Cu_3O_7}$ compounds.[22,23] By comparing the magnetic intensities with the nuclear ones, we obtain a saturated ordered moment of $\langle \mu_z \rangle = 6.98(7)\mu_B$ for the Tb ions. This value of the ordered moment is somewhat less than the Tb moment of $7.43\mu_B$ observed[11] in $\mathrm{Pb_2Sr_2TbCu_3O_7}$.

Shown in Fig. 5 is the variation of the $\{\frac{1}{2}\frac{1}{2}\frac{1}{2}\}$ peak intensity with temperature. This plot reveals a number of interesting features. (1) Although the measurements were made on a powder sample, where the critical scattering tends to broaden the apparent transition, the transition is relatively sharp; the large drop in intensity occurs within 1 K change in temperature. This transition is much sharper than the superconducting transition observed at higher temperature. We note that a sharp magnetic transition is a characteristic of 2D ordering, which is expected to occur for most of the rare-earth ordering in high-T_c oxides.[24] However, no further evidence of 2D nature was observed in the present study. (2) The ordering temperature of the Tb spins, as determined by the inflection

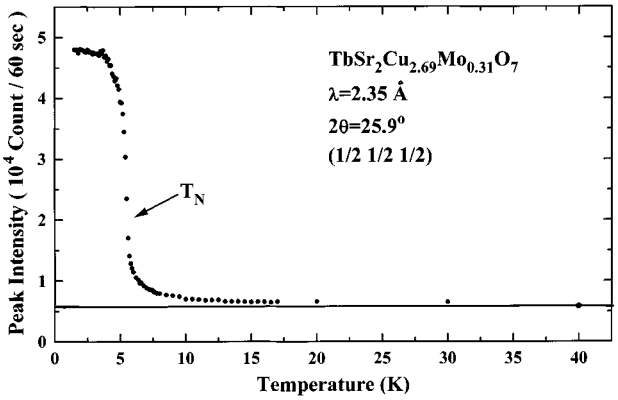

FIG. 5. Variation of the $\{\frac{1}{2}\frac{1}{2}\frac{1}{2}\}$ peak intensity with temperature, showing a $T_N \approx 5.4$ K for the Tb spins. The solid line shown at the bottom indicates the background level. The correlations between the Tb spins persist up to ~ 40 K.

point, is $T_N \approx 5.4$ K. This temperature is consistent with the position of the corresponding peak observed in $\chi''(T)$ shown in Fig. 3. (3) Above T_N the $\{\frac{1}{2}\frac{1}{2}\frac{1}{2}\}$ intensity decreases gradually, and it remains to temperatures well above T_N. The baseline shown at the bottom of Fig. 5 is the background intensity determined based on the measurements made at $40\ \text{K} \leqslant T \leqslant 60$ K (not shown). Even at $T = 30$ K the $\{\frac{1}{2}\frac{1}{2}\frac{1}{2}\}$ intensity is still above the background level. The present compound is hence an ideal system to study the effect of temperature on the correlation length of the Tb spins, even though only powder samples are available at the present time.

To isolate the magnetic signal from the nuclear one, we have employed the subtraction techniques[25] where diffraction patterns taken at high temperature are subtracted from the one taken well below T_N. Below 40 K the magnetic scattering is observed as peaks (broad or well defined). We hence use the diffraction pattern taken at 40 K as the nonmagnetic ''background,'' and apply the subtraction technique to isolate the magnetic scattering. In Fig. 6 we show the magnetic intensity thus obtained at six different temperatures, covering $5\ \text{K} \leqslant T \leqslant 30$ K. Above 40 K the magnetic intensity is angle independent, showing there are no significant Tb spin correlations. At 30 K a broad peak at the $\{\frac{1}{2}\frac{1}{2}\frac{1}{2}\}$ position becomes evident as shown in Fig. 6(f). This critical scattering originates from the short-range spin correlations among the Tb moments. We note that the bump and dip around $2\theta = 10°$ and 35° are the direct result of subtracting the {001} and {100}+{010}+{003} nuclear peaks, respectively, at two different temperatures due to the changes

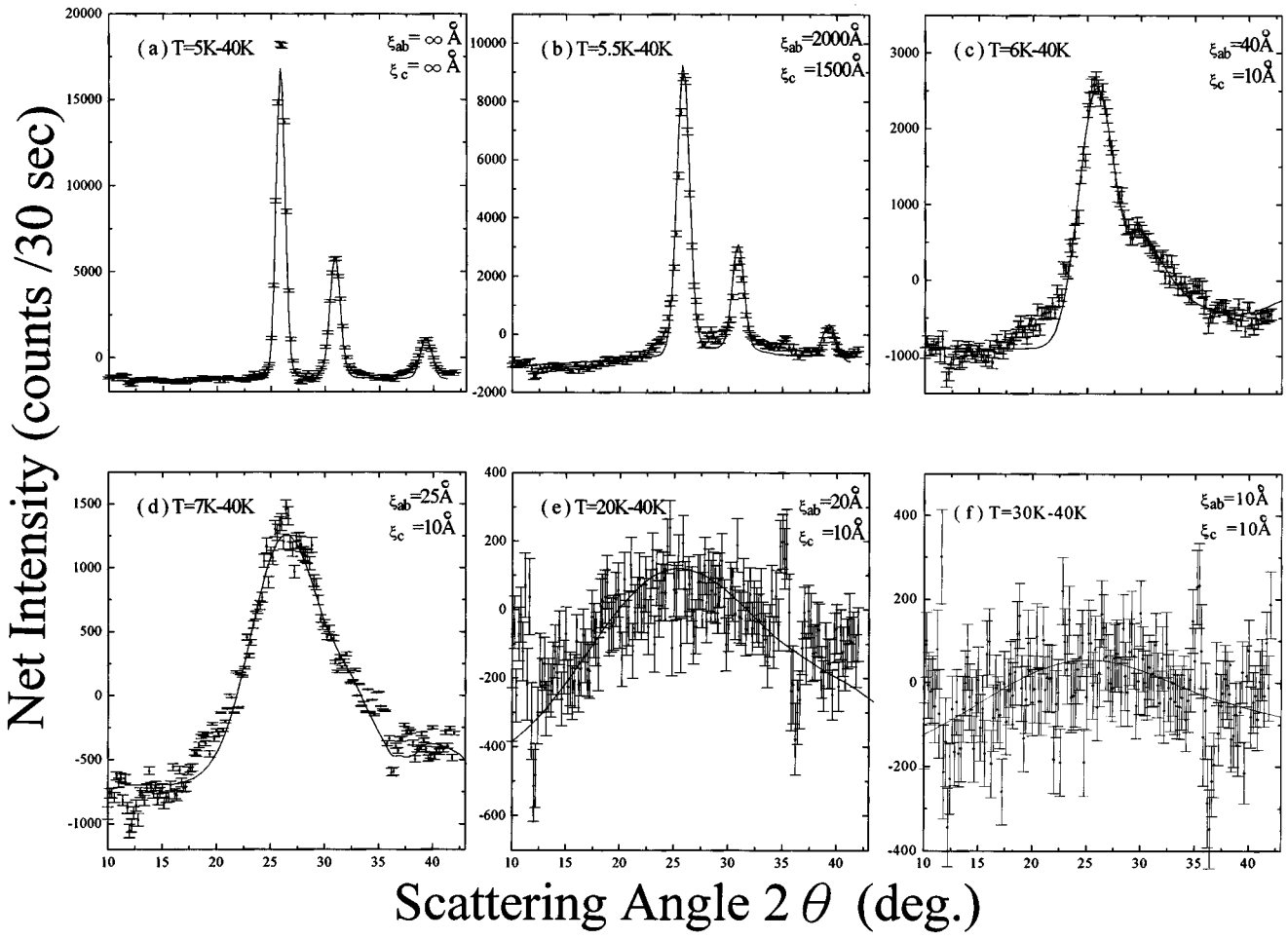

FIG. 6. Magnetic-diffraction pattern observed at six different temperatures. The magnetic scattering starts to develop into peaks below $T \approx 40$ K, and the peaks become better defined as the temperature is reduced. The solid curves shown are fits of the data to the scattering profile discussed in the text.

in lattice constants. The $\{\frac{1}{2}\frac{1}{2}\frac{1}{2}\}$ peak becomes more pronounced and better defined as the temperature is lowered. For $T \geqslant 6$ K the $\{\frac{1}{2}\frac{1}{2}\frac{1}{2}\}$ peak dominates the expected $\{\frac{1}{2}\frac{1}{2}\frac{3}{2}\}$ and $\{\frac{1}{2}\frac{1}{2}\frac{5}{2}\}$ peaks for 3D ordering, indicating the correlation length along the c axis is relatively short compared to the in-plane correlation length. Fits imposing the same value for ξ_{ab} and ξ_c give much worse results. This is understandable since the nearest-neighbor distance between the Tb ions along the c axis is three times longer than those in the ab plane. On the other hand, assuming a pure 2D system ($\xi_c = 0$) also provided an inadequate fit to the data. The solid curves shown in Figs. 6(c)–6(f) are fits of the data to the theoretical curves for 3D short-range correlations[26,27] convoluted with the Gaussian instrumental resolution function, allowing the correlation lengths within the ab plane ξ_{ab} and along the c axis direction ξ_c to take different values. As the temperature is reduced below 6 K, the intensity increases rapidly and the width narrows. At $T = 5.5$ K, as shown in Fig. 6(b), symmetrical well-defined peaks at the $\{\frac{1}{2}\frac{1}{2}\frac{1}{2}\}$, $\{\frac{1}{2}\frac{1}{2}\frac{3}{2}\}$, and $\{\frac{1}{2}\frac{1}{2}\frac{5}{2}\}$ positions become clear. The appearance of the $\{\frac{1}{2}\frac{1}{2}\frac{3}{2}\}$ and $\{\frac{1}{2}\frac{1}{2}\frac{5}{2}\}$ peaks shows that correlations along the c axis direction have developed. However, both ξ_{ab} and ξ_c, are still finite at this temperature, as the widths of the peaks are still broader than the instrumental resolutions. The solid curves shown in Fig. 6(b) are fits of the data to 3D profiles, with a larger value for ξ_{ab} than for ξ_c. At $T = 5$ K the widths of the peaks reach the instrumental resolution and the correlation lengths diverge, indicating that the Tb spins have ordered. The solid curves shown in Fig. 6(a) are fits of the data to the instrumental resolution function. We note that the ordered moment at 5 K is about 85% of the saturated moment, as can be seen from the order parameter measurements shown in Fig. 5.

V. CONCLUSION

Single phase $TbSr_2Cu_{2.69}Mo_{0.31}O_7$ that crystallizes into the well-known $YBa_2Cu_3O_7$ structure with Mo replacing the Cu in the CuO-chain layers has been successfully synthesized. Superconductivity with $T_c \approx 32$ K and antiferromagnetic order of the Tb spins with $T_N \approx 5.4$ K are observed. Although the Tb ions are located right between the two superconducting CuO_2 layers, the superconductivity remains as the Tb spins order, and superconductivity and antiferromagnetic order coexist at low temperatures. This coexistence occurs despite the high magnetic ordering temperature of the Tb spins, which is comparable to the ordering temperatures observed in the RNi_2B_2C systems.[28] In these materials the T_N is much higher than can be accounted for based on dipolar interactions, and hence the ordering must originate from exchange. For the Tb-123 system the T_N is relatively high and the correlations persist up to 40 K, in the temperature regime where superconductivity develops.

ACKNOWLEDGMENTS

The research at the NCU was supported by the National Science Council of the Republic of China under Grant No. NSC 86-2112-M-008-029. The research at the NSYSU was supported by the National Science Council of the Republic of China under Grant No. NSC 86-2112-M-110-013.

[1] For a review see G. Burns, *High-Temperature Superconductivity, An Introduction* (Academic, San Diego, 1992).
[2] L. Soderholm, C.-K. Loong, and S. Kern, Phys. Rev. B **45**, 10 062 (1992).
[3] J. W. Lynn, J. Alloys Compd. **181**, 419 (1992).
[4] U. Staub, J. Mesot, M. Guillaume, P. Allenspach, A. Furrer, H. Mutka, Z. Bowden, and A. D. Taylor, Phys. Rev. B **50**, 4068 (1994).
[5] K. N. Yang, B. W. Lee, M. B. Maple, and S. S. Laderman, Appl. Phys. A **46**, 229 (1988).
[6] U. Staub, L. Soderholm, S. Skanthakumar, and M. R. Antonio, Phys. Rev. B **52**, 9736 (1995).
[7] F. Beech, S. Miraglia, A. Santoro, and R. S. Roth, Phys. Rev. B **35**, 8778 (1987).
[8] Q. Xiong, Y. Y. Xue, J. W. Chu, Y. Y. Sun, Y. Q. Wang, P. H. Hor, and C. W. Chu, Phys. Rev. B **47**, 11 337 (1993).
[9] H. L. Tsay, C. R. Shih, Y. C. Chen, W. H. Lee, T. H. Meen, and H. D. Yang, Physica C **252**, 79 (1995).
[10] T. Den and T. Kobayashi, Physica C **196**, 141 (1992).
[11] S. Y. Wu, W. T. Hsieh, W-H. Li, K. C. Lee, J. W. Lynn, and H. D. Yang, J. Appl. Phys. **75**, 6598 (1994).
[12] S. Y. Wu, W-H. Li, K. C. Lee, J. W. Lynn, T. H. Meen, and H. D. Yang, Phys. Rev. B **54**, 10 019 (1996).
[13] F. Beech, S. Miraglia, A. Santoro, and R. S. Roth, Phys. Rev. B **35**, 8778 (1987).
[14] A. C. Larson and R. B. von Dreele (unpublished).
[15] H. M. Rietveld, J. Appl. Crystallogr. **2**, 65 (1969).
[16] R. A. Young edited, *The Rietveld Method* (Oxford University Press, New York, 1993).
[17] S. W. Lovesey, *Theory of Neutron Scattering from Condensed Matter* (Clarendon, Oxford, 1984).
[18] J.-H. Müller and A. J. Pauza, Physica C **161**, 319 (1989).
[19] S. L. Shindw, J. Morrill, D. Goland, D. A. Chance, and T. McGuire, Phys. Rev. B **41**, 8838 (1990).
[20] A. Kompany, Y. J. Qian, M.-F. Xu, H-P. Baum, W. Willman, and M. Levy, Solid State Commun. **75**, 579 (1990).
[21] M. Mehbod, S. Sergeenkov, M. Ausloos, J. Schroeder, and A. Dang, Phys. Rev. B **48**, 483 (1993).
[22] W-H. Li, J. W. Lynn, S. Skanthakumar, T. W. Clinton, A. Kebede, C.-S. Jee, J. E. Crow, and T. Mihalisin, Phys. Rev. B **40**, 5300 (1989).
[23] K. N. Yang, J. M. Ferreira, B. W. Lee, M. B. Laple, W.-H. Li, J. W. Lynn, and R. W. Erwin, Phys. Rev. B **40**, 10 963 (1989).
[24] J. W. Lynn, J. Alloys Compd. (to be published).
[25] Details can be found in J. W. Lynn, J. A. Gotaas, R. N. Shelton, H. E. Horng, and C. J. Glinka, Phys. Rev. B **31**, 5756 (1985).
[26] H. Zhang, J. W. Lynn, W-H. Li, T. W. Clinton, and D. E. Morris, Phys. Rev. B **41**, 11 229 (1990).
[27] W-H. Li, W. T. Hsieh, and K. B. Lee, J. Phys. B **7**, 6513 (1995).
[28] J. W. Lynn, S. Skanthakumar, Q. Huang, S. K. Sinha, Z. Hossain, L. C. Gupta, R. Nagarajan, and C. Godart, Phys. Rev. B **55**, 6584 (1997).